



# Bionic design of universal gripper for nursing robot with hybrid joints and variable Equivalent Link Length

Dingmin Xu<sup>1</sup> · Xueyong Li<sup>1</sup> · Yonghui Wang<sup>2</sup>

Received: 30 January 2022 / Accepted: 7 November 2022 / Published online: 24 November 2022  
© The Author(s), under exclusive licence to The Brazilian Society of Mechanical Sciences and Engineering 2022

## Abstract

Currently, most rehabilitation/nursing robots attach the human body to the end of the robot by ‘binding’ solution, which makes the operation complicated and greatly limits their applications. Therefore, it is necessary to study a universal gripper that can directly grasp human limbs as the end-effector of the robot. Inspired by the human hand, this paper proposes a bionic under-actuated gripper that imitates the structure of human hand. The concept of Equivalent Link Length (ELL) is proposed to optimize the envelope effect. And the structure with hybrid rotational and translational joints is proposed to increase gripping stiffness and to avoid the harmful component in the grip force. Theoretical analyses and experiments on envelope effect, force distribution and load capacity show that the propose gripper can grasp cylindrical (limb-shaped) objects with wide applicable size range, and also has a high load capacity. Furthermore, the gripper has the characteristic of almost constant force transfer ratio, which reduces the number of sensors required by the system. These results show that the gripper has the potential to be used in the nursing robot system.

**Keywords** Universal gripper · Variable Equivalent Link Length (ELL) · Under-actuated · Rope drive · Human limb

## 1 Introduction

In 2020, the COVID-19 pandemic has become a nightmare for people all over the world. In the process of fighting against the virus, medical staff, including nurses and rehabilitation therapists, are suffering the risk of infection and under the great pressure of physical labor intensity [1]. At the same time, the world is facing the problem of nursing staff shortage. Therefore, it is an urgent task to develop a nursing robot that can replace nursing staff for the nursing of COVID-19 patients [2].

As with nursing the long-term bedridden patients, there are many nursing tasks that can be completed by robots in the nursing process of the COVID-19 patients, such as bed transferring, turning over, physical rehabilitation exercises and other heavy and repetitive exercises. To complete the above nursing work, an essential operation is to use human hands to grasp the patient's limbs (i.e., legs, ankles). Therefore, the research of general-purpose end effectors which directly attach to the human body becomes an indispensable part of the whole robot system.

In the existing nursing robot system, the end effectors can be mainly divided into two categories. One is the object-oriented gripper, which is used to operate various tools used in the nursing operation, such as tableware, drugs or medical devices. The end effector of this kind of robot is no different from the ordinary gripper. For example, the dual-arm nursing robot invented by Yang [3] during the COVID-19 pandemic period used a two-finger gripper to grasp medicine or other medical necessities, or attached a Doppler ultrasound stethoscope to the end of the robot arm to assist or replace nursing staff to complete nursing work in the isolation ward. Park [4] connected the tableware to the end of a general manipulator and built a feeding robot. With camera, sensors and food position estimation algorithm, it can automatically

---

Technical Editor: Rogério Sales Gonçalves.

---

✉ Xueyong Li  
mechsd@163.com

✉ Yonghui Wang  
yonghuiw6606@126.com

<sup>1</sup> Key Laboratory of High-efficiency and Clean Mechanical Manufacture of MOE, National Demonstration Center for Experimental Mechanical Engineering Education, School of Mechanical Engineering, Shandong University, 17923 Jingshi Road, Jinan 250061, China

<sup>2</sup> Rehabilitation Center, Qilu Hospital of Shandong University, Jinan 250012, Shandong, China

shovel food and put it into the user's mouth. An automatic drinking assistant robot built by Schroer [5] used Schunk three-finger hand to control a cup to complete the feeding task of liquid food. The other category of nursing robot takes the human trunk or limbs as the target. At present, most of these researches are realized by 'binding' (tying the limbs to the end of the robot) or customized solutions. For example, Mohanta [6] introduced a mechanical arm for lower limb rehabilitation, in which the mechanical arm and the human body are fixed in a way similar to placing the limb in a customized long slot, and it needs to be combined with 'binding' methods to prevent the limb from falling; The RIBA nursing assistant robot invented by Ding [7, 8] used double arms to assist the patients with bed transferring. At the same time, a musculoskeletal model was developed to reduce the load, and a softness distribution model of the human body was created to control the robot to contact the human body at a softer place. Recently, a new implementation of nursing/rehabilitation robots using universal mechanical arm has been introduced [9, 10]. In the new scheme, the human limbs are fixed to the end of the robot hand and the passive or active rehabilitation training is carried out by imitating the manual operation. This implementation can be suitable for various rehabilitation movements without being affected by the structure of the robots or the limbs. Compared with the existing nursing/rehabilitation robots, this implementation has better flexibility and universality, and the structure is also simpler.

In brief, either the end traction [11] or the wearable exoskeleton [12–14] nursing robots are mostly based on the 'binding' solutions, that is, limbs of the human body are tied to the actuator at the end of the mechanical arm through a 'binding' device. Although this kind of solution has the advantages of safety and reliability, it also causes the problems of complicated procedures and poor adaptability. And also, limited by this fixing method, some rehabilitation exercises cannot be realized [10].

Therefore, it is of great significance to design a universal gripper that can directly grasp human limbs to complete rehabilitation or nursing operations. Different from the object-oriented gripper, the following issues should be considered as additional requirements for human body-oriented grippers: (1) The object is close to cylinder and is non-rigid, which is easy to deform and makes the gripping unstable; (2) The applicable size range for the gripper and the load capacity should be large to adapt different sizes of human limbs; (3) The structure and the control system should be simple, and the weight of the system should be light; (4) To avoid any injury to the human body, the stress concentration in the object should be as homogenized and as small as possible.

Inspired by the structure of the human hand, and the operation law when a hand gripping cylindrical objects with different radius, we proposed a novel two-finger under-actuated

grripper driven by a single rope. The gripper has a bionic structure with wide Equivalent Link Length (ELL) variation range and a hybrid of rotational and translational joints. This unique design ensures that the gripper has the advantages of wide applicable size range and high load capacity, while the structure and control system is relatively simple.

The main contributions of this paper include: (1) The concept of variable ELL is proposed to optimize the applicable size range and envelope effect of the gripper, and a novel bionic design is proposed for the realization of variable ELL. (2) A gripper with two translational joints and four rotational joints is proposed. Compared to the gripper with only rotational joints, the proposed design increases gripping stiffness and avoids the harmful component in the grip force.

The rest of this paper is arranged as follows. Section 2 summarizes the related works. Section 3 presents the bionic design for the gripper. Section 4 introduces the theoretical analysis of the gripper model. Section 5 carries out the experiments and gives the experimental result analysis. Conclusions are drawn in Sect. 6.

## 2 Related works

With the extensive application of robotics in industry, various end effectors have been proposed for different tasks. Among them, rope-driven (tendon-driven) dexterous hand and gripper with two to three fingers are widely studied, which are also related to the research in this paper. Therefore, the following part is a summary of these studies.

Because most work can be carried out by human hands, it seems that using a dexterous hand as the end effector is a feasible solution. However, the dexterous hand generally has more than a dozen joints [15], making them too complicated to build and control. Also, the dexterous hand has low flexibility and is not conducive to the lightweight design. Therefore, some novel driving methods based on the concept of under-actuated are proposed. He [16] and Rahman [17] proposed an under-actuated bionic hand driven by rope. This structure can benefit the gripper with flexibility close to the human hand without increasing the complexity of the control system. Apart from the rope-driven architecture, various driven architectures have been proposed for the under-actuated gripper. For example, Deimel [18] introduced a flexible bionic hand driven by compressed air which can improve the flexibility and reduce the complexity of the control system of the gripper. Experimental results show that the effective dimensionality of grasp postures exceeds the dimensionality of the actuation signals, which means the gripper has good flexibility and can reduce the complexity of the control system. However, due to its low load capacity, it is only suitable for gripping small and fragile objects. Daniel [19] introduced a dexterous hand with piezoelectric

brake on its joints which can lock single joint independently. The stiffness is consequently improved and the controllability is increased without increasing the number of motors. Although the complexity of these grippers is lower than the fully actuated grippers, the excessive degrees of freedom and actuators are still too complex for practical applications. Some documents point out that two to three fingers can complete most of the work done by a human hand. Therefore, many grippers with fewer fingers have been proposed. For example, the velo gripper proposed by Ciocarlie [20] is an under-actuated two-finger gripper with two + two rotational joints driven by rope, Heidari [21] proposed an under-actuated two-finger gripper with two + three rotational joints. Dong [22] studied the optimization design of a rope-driven two-finger gripper with three + three rotational joints. Except for rope drive and under-actuated, the common feature of these kinds of grippers is that all joints are rotational joints.

This kind of fully rotational joints gripper has many disadvantages, either low stiffness or the harmful components contained in the grip force. As shown in Fig. 1a, there is a force amplification phenomenon caused by the Lever Principle in the rotational joint, which means a small load force may require a large tension to counteract, and results in the gripper's poor ability to resist load changes in horizontal direction. This phenomenon is especially significant when multiple joints share a single driving rope. As shown in Fig. 1b, when the two internal joints rotate in the direction indicated by the arrow, the grip force between the Internal Link and the object contains harmful components, which may push the object away from the gripper.

Some grippers are designed for homogenizing the stress in the object, such as the flexible gripper based on pneumatic inflation. The grippers with inflatable rubber bag [23] or with magnetic fluid bag [24] all have a good homogenization effect on the stress distribution in the object. However, these kind of grippers are mainly suitable for gripping small objects. When it comes to a larger object, the mass and volume of the inflatable bag will increase to an unacceptable magnitude.

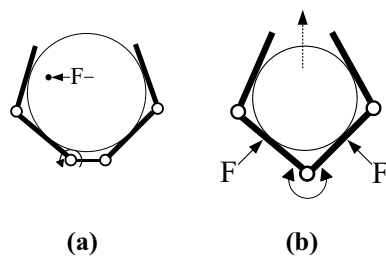


**Fig. 1** Disadvantages of fully rotational joints gripper. **a** The gripping stiffness is low in the horizontal direction. **b** The grip force contains harmful components

### 3 Bionic design and Effective Link Length

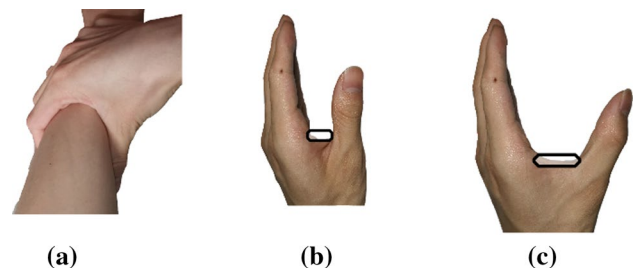
#### 3.1 Analysis of hand structure when nursing workers gripping human limbs

Figure 2 shows the structural characteristics when human hands gripping objects with different sizes. Figure 2a is the picture of a nurse gripping human limbs during nursing operation. The limb is surrounded by the thumb and index finger. In the process, the hand looks like it is wearing a mitten, which is characterized by separating the thumb on one side and encasing the other four fingers together on the other side. When gripping, the four fingers move together to form a wider 'finger', in a shape that actually increases the area of contact.

Figure 2b,c respectively shows the hand gripping objects with medium-size and large-size. It can be seen that the shape of the fingers has hardly changed, but the distance between the thumb and the index finger in translational direction has changed. The V-shaped area between thumb and index finger forms as a straight line in the horizontal direction, which actually plays the role of a translational joint. This avoids the disadvantages of fully rotational joints grippers, such as the low stiffness and the harmful components contained in the grip force.

As shown in Fig. 3a,b, when the finger is bending, the tendon pulls the skin away from the bones, and skinfolds accumulate at the joints. This results in a smaller link length seen from the object (in the figure, look from the right to the left). As shown in Fig. 3(c), the link length  $e_1, e_2, e_3$ , which differs from the physical length of the link  $a_1, a_2, a_3$ , varies with the bending angle  $\theta_2, \theta_3$  and is defined as the Effective Link Length (ELL). The ELL of three links are equal to the physical length  $a_1, a_2, a_3$  only when  $\theta_2$  and  $\theta_3$  are 0. The specific relationship among ELL, physical length and bending angle will be given in Sect. 4.

Figure 4 shows the sketch of the grippers when gripping objects with different radius (as in rows 1 and 2). The structures with three different configurations of rotational



**Fig. 2** Structural characteristics of human hand when gripping objects. **a** Gripping human limb by hands. **b** Gripping medium-size objects and **c** large-size objects by hand

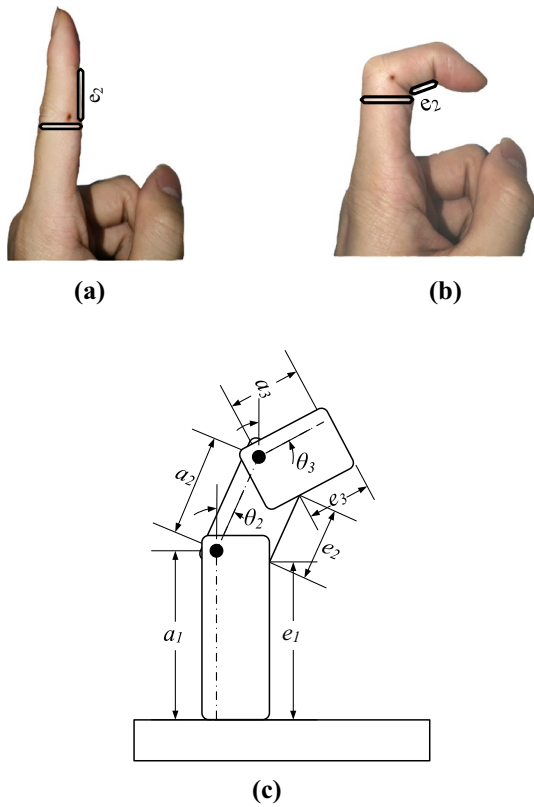


**Fig. 3** Changes of Equivalent Link Length (ELL) of human fingers in **a** straight state and **b** bending state. And **c** the symbols used in the ELL analysis

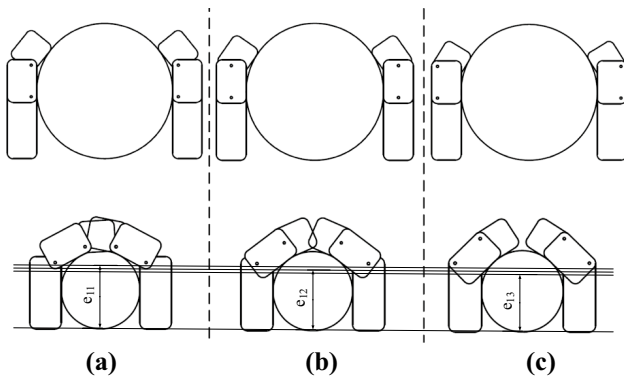


**Fig. 4** Envelope effect of gripper with **a** small **b** medium and **c** large Equivalent Link Length (ELL) variation range

joints (as in columns 1,2,3) have the same physical length of the links, except that the locations of the rotational joints are different. The third column (c) is the bionic structure in line with the human hand. Taking  $e_1$  as an example, the relationship of  $e_1$  corresponding to three structures is  $e_{11} > e_{12} > e_{13}$ , and the relationship of ELL variations  $a - e$  is  $(a_1 - e_{11}) < (a_1 - e_{12}) < (a_1 - e_{13})$ . It

can be seen that if the object is large as shown in row 1 of Fig. 4, there are no significant difference in the envelope effect for all the three structures. However, if the object is small, the structures with small ELL variation (Fig. 4a,b) encounter obvious interference, which reduces the applicable size range for the gripper. But the third column with large ELL variation (Fig. 4c) has no interference and can grasp normally.

### 3.2 Bionic concept and structure design

Inspired by the structural characteristics of the human hand, we propose a single rope under-actuated gripper, which is characterized by the hybrid of rotational joint and translational joint, and the application of variable ELL based on the bionic structure. The mechanism schematic diagram is shown in Fig. 5.

Same as Fig. 4c, it can be seen that the rotational joint is far away from the object, and the joints and links are separated from the rope, which can simplify the structure and have a large ELL variation range. In addition, the structure has the following characteristics:

- (1) Compared with the traditional fully rotational joint gripper as shown in Fig. 1, this design can avoid the harmful components contained in the grip force which can push the object away from the gripper. This kind of gripper with spring and torsion spring can carry out a better self-centering envelope and has a wider applicable size range.
- (2) The single rope under-actuated architecture has the advantages of simple structure and lightweight, and more importantly, it can coordinate the driving force of each joint with the load force without the active intervention of the control system, and can effectively homogenize the stress in the object.

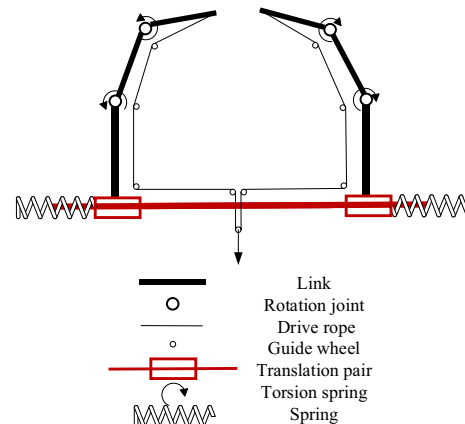


**Fig. 5** The mechanism schematic diagram of the design

### 4 Theoretical analysis

The gripper designed according to the schematic diagram of Fig. 5 is shown in Fig. 6. Because the human limbs are almost cylindrical, we assumed the gripper grips a cylindrical object. Due to the existence of variable ELL, the D-H method cannot be used for theoretical calculation. In this paper, the whole system is projected to the plane perpendicular to the axis of the cylinder, and the dimension diagram of the bionic gripper as shown in Fig. 6 is obtained. A XOY coordinate system is established at the center of the object to carry out the theoretical analysis. The symbols and their definitions used in the theoretical analysis are listed in Table 1.

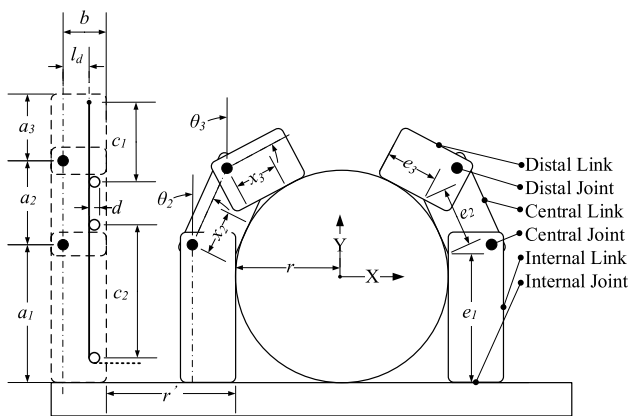


Fig. 6 Structure and dimension diagram of the bionic gripper

#### 4.1 Relationship among Equivalent Link Length, joint movement and the radius of the object

To evaluate the envelope effect of the gripper, the relationship among Equivalent Link Length (ELL) ( $e_1, e_2, e_3$ ), joint movements ( $r', \theta_2, \theta_3$ ) and the radius of the object  $r$  is derived. From the geometric relationship shown in Fig. 6, the relationship can be obtained as shown in Equations (1)-(4). Where  $c$  is a constant.

$$r' = c - r \tag{1}$$

$$\frac{a_1 \tan \theta_2 + b(1 - \sqrt{1 + \tan^2 \theta_2})}{\tan \theta_2 - 1 + \sqrt{1 + \tan^2 \theta_2}} \theta_2 = r \tag{2}$$

$r', \theta_2$  can be solved. And substitute  $\theta_2$  into Eq. (3) to solve  $\theta_3$ .

$$\frac{a_1 \tan \theta_3 + b(1 - \sqrt{1 + \tan^2 \theta_3}) + a_2(\cos \theta_2 \tan \theta_3 - \sin \theta_2)}{\tan \theta_3 - 1 + \sqrt{1 + \tan^2 \theta_3}} = r \tag{3}$$

The ELL can be solved by introducing  $\theta_2$  and  $\theta_3$  into Eq. 4.

$$\begin{bmatrix} e_1 \\ e_2 \\ e_3 \end{bmatrix} = \begin{bmatrix} a_1 \\ a_2 \\ a_3 \end{bmatrix} + \begin{bmatrix} -b & 0 \\ -b & -b \\ 0 & -b \end{bmatrix} \times \begin{bmatrix} \tan \frac{\theta_2}{2} \\ \tan \frac{\theta_3}{2} \end{bmatrix} \tag{4}$$

Taking the radius of the object  $r$  as the variable, the ELL of each link  $e_1, e_2, e_3$  and the ratio of ELL  $\frac{e_1}{a_1}, \frac{e_2}{a_2}, \frac{e_3}{a_3}$  are obtained from the Eqs. (1)-(4).

Table 1 Symbols used in theoretical analysis

Symbol	Description	Value
$a_1, a_2, a_3$	Physical length of the links (mm)	60,38,30
$b$	ELL structure parameter (mm)	26
$l_d$	Rope location parameter (mm)	13
$c_1, c_2$	Guide wheel location parameter (mm)	29, 85
$d$	Diameter of the guide wheel (mm)	12
$k_1$	Linear stiffness of the springs of Internal Joint (N/mm)	0.9
$k_2, k_3$	Rotational stiffness of the springs of Central Joint and Distal Joint (N·mm/rad)	0, 80
$F'$	Preload force of the spring of Internal Joint (N)	10
$M'_2, M'_3$	Preload moment of the springs of Central Joint and Distal Joint (N·mm)	20, 40
$r'$	Movement of joints when gripping (mm)	
$\theta_2, \theta_3$	Movement of joints when gripping (radian)	
$r$	Radius of the object (mm)	
$x_2, x_3$	Arm of the grip force between each link and the object or the coordinate of the contact position (mm)	
$e_1, e_2, e_3$	ELL of each link (mm)	
$f$	Tension of the driving rope (N)	
$F_l$	Load capacity of the gripper (N)	
$\mu$	Friction coefficient	



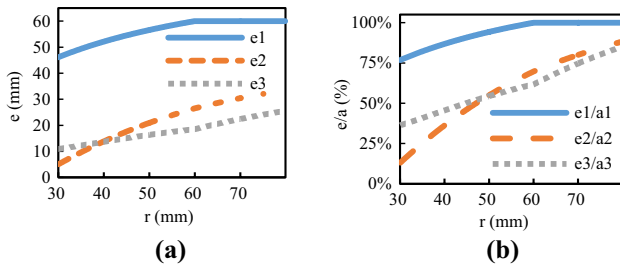


**Fig. 7** The relationship between the radius of the object and **a** the Equivalent Link Length (ELL), **b** the ratio of ELL

The relationships between the radius of the object and the Equivalent Link Length ( $e_1, e_2, e_3$ ), and the relationships between the radius of the object and the ratio of ELL ( $\frac{e_1}{a_1}, \frac{e_2}{a_2}, \frac{e_3}{a_3}$ ) are respectively listed in Fig. 7a,b. The abscissa is the radius of the object, and the ordinate is the ELL and ratio of ELL of each link.

From the figures, the following conclusions can be drawn:

(1) The ELL of each link increases with the increase in the radius of the object, and the variation of  $e_2$  is much larger than  $e_1$  and  $e_3$ . The reason is that  $e_2$  is affected by both  $\theta_2$  and  $\theta_3$ , as shown in Eq. (4).

(2) The ratio of ELL of each link increases with the increase in the radius. When the radius is small, the ratio of ELL can be as low as 77%, 15%, and 37%, respectively. It shows that the gripper can dynamically adjust its ELL according to the size of the object. This characteristic can increase the applicable size range for the gripper and improve the envelope effect.

(3) When the radius of the object is greater than 60 mm,  $e_1$  and  $\frac{e_1}{a_1}$  stop changing, this is because the radius is greater than  $a_1$ , and the object is no longer in contact with the Internal Link.

### 4.2 Relationship between rope tension and grip force

To study the load capacity of the gripper and the stress concentration effect in the object, it is necessary to derive the relationship between the rope tension and the grip force exerted to the object by each link. According to the geometric relationship shown in Fig. 6, the arm of the grip force (also the coordinate of the contact position) between Internal Link and the object does not change. However, the arm of the grip force of Central Link  $x_2$  and Distal Link  $x_3$  change with the radius of the object and can be obtained by Eq. (5) and Eq. (6):

$$x_2^2 = \left( b + r - \frac{b + r + a_1 \tan \theta_2 - r \tan \theta_2}{1 + \tan^2 \theta_2} \right)^2 + \left( r - a_1 + \tan \theta_2 \frac{b + r + (a_1 - r + a_2 \cos \theta_2) \times \tan \theta_3 - a_2 \sin \theta_2}{1 + \tan^2 \theta_3} \right)^2 \tag{5}$$

$$x_3^2 = \left( a_1 - r + a_2 \cos \theta_2 - \tan \theta_3 \times \frac{b + r + (a_1 - r + a_2 \cos \theta_2) \times \tan \theta_3 - a_2 \sin \theta_2}{1 + \tan^2 \theta_3} \right)^2 + \left( b + r - a_2 \sin \theta_2 - \frac{b + r + (a_1 - r + a_2 \cos \theta_2) \times \tan \theta_3 - a_2 \sin \theta_2}{1 + \tan^2 \theta_3} \right)^2 \tag{6}$$

According to the geometric relationship shown in Fig. 6, the grip force of each link can be obtained as shown in Eqs. (7)-(12), where  $F$  is the grip force,  $M$  is the driving torque for each link. Subscript  $IL$  refers to the Internal Link,  $CL$  refers to the Central Link,  $DL$  refers to the Distal Link. Superscript  $'$  and  $''$  refers to intermediate variable.

The  $F_{DL}$  and  $F'_{CL}$  can be solved by introducing  $\theta_2, \theta_3$  and  $f$  into the following Eqs. (7)-(10).

$$F'_{DL} x_3 = M'_{DL} = -M'_3 + l_d f \cos(\theta_3 - \theta_2) - k_3(\theta_3 - \theta_2) \tag{7}$$

$$F''_{CL} x_2 = M''_{CL} = -M'_2 + M'_3 + l_d f \cos \theta_2 - k_2 \theta_2 - (F'_{DL} a_2 + l_d f) \cos(\theta_3 - \theta_2) + k_3(\theta_3 - \theta_2) \tag{8}$$

However, the grip force must not be smaller than 0. To make sure  $F_{CL} \geq 0$ , the maximum value of  $F_{DL}$  (mark as  $F''_{DL}$ ) can be solved by setting  $F''_{CL}$  and  $M''_{CL}$  as 0 and replaced  $F'_{DL}$  with  $F''_{DL}$  into the following Eqs. (11)-(12)

$$0 = -M'_2 + M'_3 + l_d f \cos \theta_2 - k_2 \theta_2 - (F''_{DL} a_2 + l_d f) \cos(\theta_3 - \theta_2) + k_3(\theta_3 - \theta_2) \tag{9}$$

$$[F_{DL}, F'_{CL}] = \begin{cases} [F'_{DL}, F''_{CL}] & F'_{DL} < F''_{DL} \\ [F''_{DL}, 0] & F'_{DL} > F''_{DL} \end{cases} \tag{10}$$

$F_{CL}$  and  $F_{IL}$  can be solved by introducing  $\theta_2, \theta_3, f$  and  $F'_{CL}$  into the following Eqs. (11)-(12).

$$F'_{IL} = f - F' - k_1 m - F'_{CL} \cos \theta_2 - F_{DL} \cos \theta_3 \tag{11}$$

When the radius of the object  $r$  is greater than  $a_1, \theta_2$  will be 0 and the Internal Link no longer contacts with the object. At this time, due to the function of the position-limit mechanism, the Central Link replaces the Internal Link to bear the grip force.  $F_{IL}$  will be 0 and  $F_{CL}$  will be the largest value of  $F'_{IL}$  and  $F'_{CL}$ .

$$[F_{CL}, F_{IL}] = \begin{cases} [F'_{CL}, 0] & (\theta_2 = 0, F'_{IL} < F'_{CL}) \\ [F'_{IL}, 0] & (\theta_2 = 0, F'_{IL} > F'_{CL}) \\ [F'_{CL}, F'_{IL}] & (\theta_2 \neq 0) \end{cases} \tag{12}$$

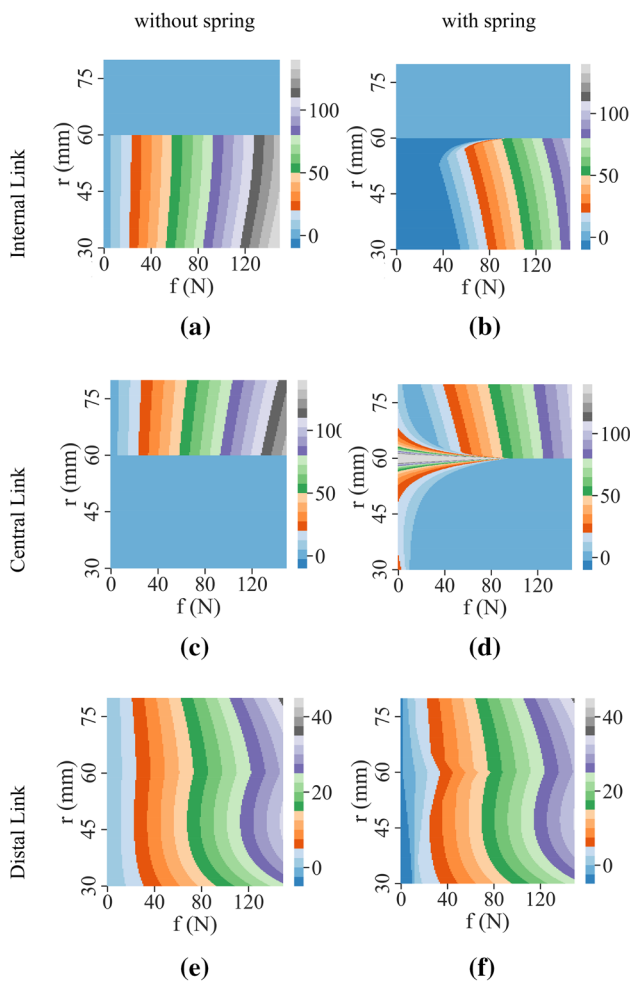


**Fig. 8** The relationship among rope tension (abscissa,  $f$  (N)), object radius (ordinate,  $r$  (mm)), grip force (color, N) of Internal, Central, Distal link (first, second, third row) without spring (Left column) or with spring (right column)

Take the radius of the object  $r$  and the rope tension  $f$  as variables, and take the friction coefficient  $\mu$  as 0.

Regardless the influence of springs (taking  $k_1, k_2, k_3, F', M'_2, M'_3$  as 0), the relationship among rope tension, object radius, grip force of each link corresponding to Eqs. (7)-(12) are respectively shown in Fig. 8a, c, e.

Considering the influence of springs, the springs parameters are shown in Table 1 ( $k_1=0.9$  N/mm,  $k_2=0$  N·mm/rad,  $k_3=80$  N·mm/rad,  $F'=10$  N,  $M'_2=20$  N·mm,  $M'_3=40$  N·mm), the relationship among rope tension, object radius, grip force of each link corresponding to Eqs. (7)-(12) are respectively shown in Fig. 8b,d,f.

In the figure, the abscissa is the rope tension  $f$ , the ordinate is the radius of the object  $r$ , and the grip force is represented with the color in the color bar on the right of each subgraph.

From Fig. 8, the following results can be obtained:

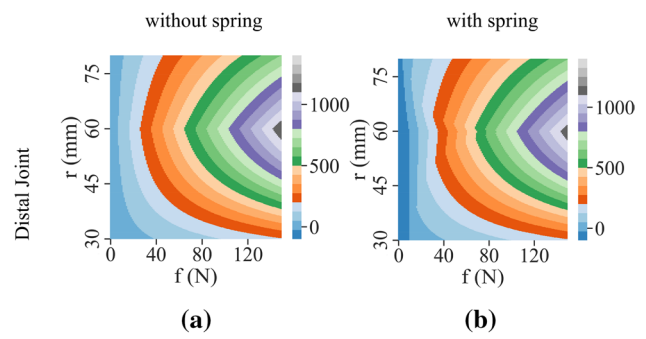


**Fig. 9** The relationship among rope tension (abscissa,  $f$  (N)), object radius (ordinate,  $r$  (mm)), driving torque (color, N·mm) of Distal Joint without spring (Left column) or with spring (right column)

1) Whether or not considering the influence of the springs, the grip force generally increases with the decrease in the radius of the object and the increase in the rope tension. When the radius of the object  $r$  is greater than 60 mm, the grip force  $F_{IL}$  of the Internal Link is 0. The reason is that the Internal Link no longer contacts with the object when  $r$  is greater than  $a_1$ . Therefore, due to the function of the position-limit mechanism, the Central Link replaces the Internal Link to bear the grip force, as shown in Fig. 8a, c.

2) As shown in Fig. 8d, when the radius of the object  $r$  is close to 60 mm, the arm of the grip force  $x_2$  and  $x_3$  are close to 0, which makes the grip force becomes infinite, and results in a rounding error.

3) As shown in Fig. 8b,d,f, when the rope tension  $f$  is small, the grip force may be less than 0. This is because the driving force acting on each joint is less than the spring prestress.

Figure 8 shows the relationship among rope tension, object radius, driving torque of Distal Joint without or with spring. In the figure, the abscissa is the rope tension  $f$ , the ordinate is the radius of the object  $r$ , and the driving torque of Distal Joint is represented with the color in the color bar on the right of each subgraph.

As shown in Fig. 8e,f and Fig. 9a,b, due to the existence of the arm of force ( $l_d \cos \theta_2, l_d \cos(\theta_3 - \theta_2)$ ) of rope tension  $f$  in Eqs. (8)-(10), when the radius, when the radius of the object changes, the driving torque of each joint changes greatly. However, the arm of the grip force of each link  $x_2$  and  $x_3$  also change. As a result, the grip force is basically unchanged. This characteristic indicates that the gripper has a relatively constant force transfer ratio, which makes it possible to obtain the pressure at all contact points by using only one rope tension sensor. This characteristic helps to reduce the weight and the complexity of the system.

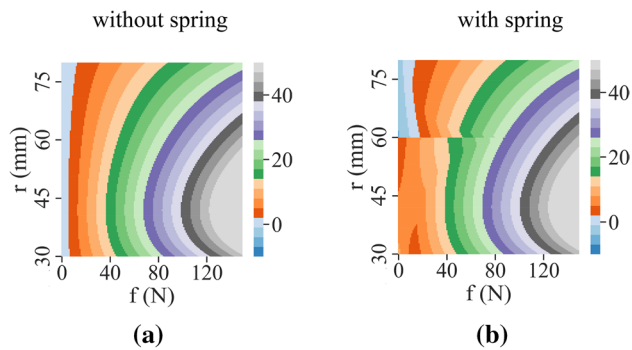


**Fig. 10** The relationship among rope tension (abscissa,  $f$  (N)), object radius (ordinate,  $r$  (mm)), load capacity (color, N) without spring (Left column) or with spring (right column)

### 4.3 Relationship between rope tension and load capacity

The load capacity refers to the maximum weight the gripper can grasp, which is an important indicator in evaluating nursing robots. The load capacity is determined by the rope tension  $f$ . It is important to study the relationship between the load capacity and the rope tension for verifying the rationality of the gripper. The load capacity is partly provided by the component of the grip force, and the other part is provided by the friction force derived from the grip force. The relationship between the load capacity and the grip force of each link is shown in Eq. (13).

$$F_l = 2F_{DL}(\sin \theta_3 + \mu \cos \theta_3) + 2F_{CL}(\sin \theta_2 + \mu \cos \theta_2) + 2\mu F_{IL} \quad (13)$$

In which,  $F_l$  is the load capacity,  $F_{IL}, F_{CL}, F_{DL}$  are respectively the grip force of each link and can be calculated by Equations (7)-(12). The radius of the object  $r$  and the rope tension  $f$  are taken as variables, and the friction coefficient is taken as 0.

From Eq. (1), the relationship among rope tension, object radius, load capacity of the gripper without or with spring is respectively shown in Fig. 10a and Fig. 10b. In the figure, the abscissa is the rope tension  $f$ , the ordinate is the radius of the object  $r$ , and the load capacity is represented with the color in the color bar on the right of each subgraph. From Fig. 10, the following results can be obtained:

1) As shown in Fig. 10, the load capacity is always greater than 0, which shows that the grip force of each link has no harmful component to push the object away from the gripper. This is because the angles  $\theta_2$  and  $\theta_3$  all vary from 0 to  $\frac{\pi}{2}$ , so that all coefficients of the grip force of each link ( $F_{DL}, F_{CL}, F_{IL}$ ) in Eq. (13) are not less than 0.

2) The load capacity is most affected by the rope tension. When the rope tension increases, the load capacity

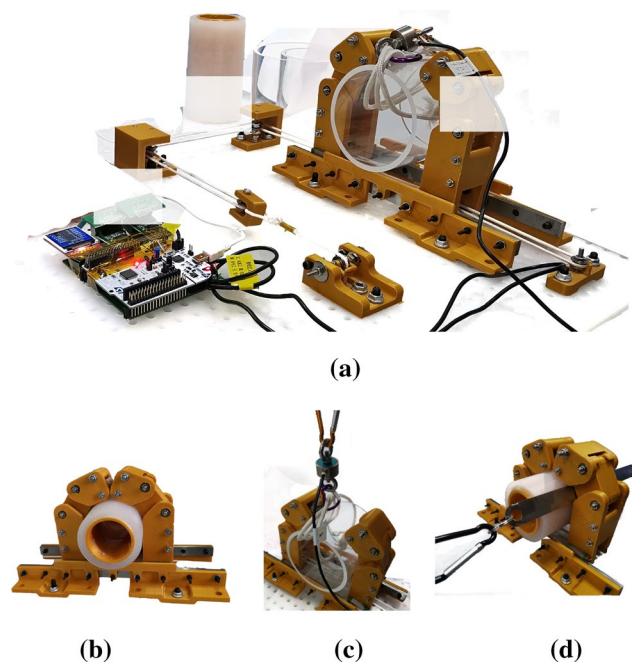


**Fig. 11** The experimental setup and experimental process. **a** The experimental setup, where part i is the bionic gripper, part ii is the objects to be grasped, part iii is the data measurement and acquisition system. **b** The gripper is grasping a non-rigid object. And **c** indicates the experimental process to verify the load capacity, and **d** indicates the experimental process to verify the grip force

increases greatly. When the radius of the object increases, the coefficients of grip force of each link ( $F_{DL}, F_{CL}, F_{IL}$ ) in Eq. (13) will change, but the grip force obtained from Eqs. (7)-(12) will change at the same time and partially cancel out the change of the coefficients, resulting in a stable load capacity. When the radius of the object  $r$  is close to 60 mm, the same rounding-off error as Fig. 8 occurs. The reasons are the same as mentioned in Sect. 4.2.

3) When the rope tension is small, the spring has a significant effect on the load capacity. When the rope tension increases to a large value, the influence of the spring becomes relatively small.

## 5 Experimental verification and discussion

### 5.1 The experimental setup

In order to verify the theoretical model, the experimental system as shown in Fig. 11a is constructed. The system consists of three parts: the bionic gripper (part i), the objects to be grasped (part ii) and the data acquisition system (part iii). The bionic gripper is composed of the framework manufactured by 3D printing, bearing, guide rail and other standard parts.



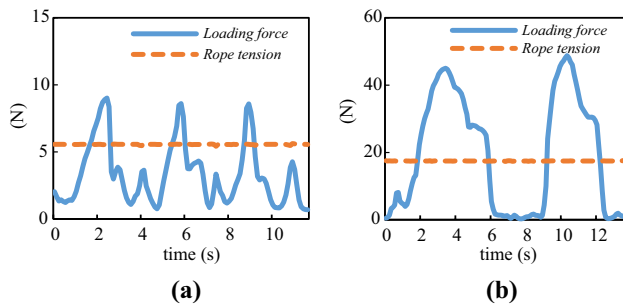


**Fig. 12** The original data collected in the experimental process on **a** the rigid acrylic object and on **b** the non-rigid object

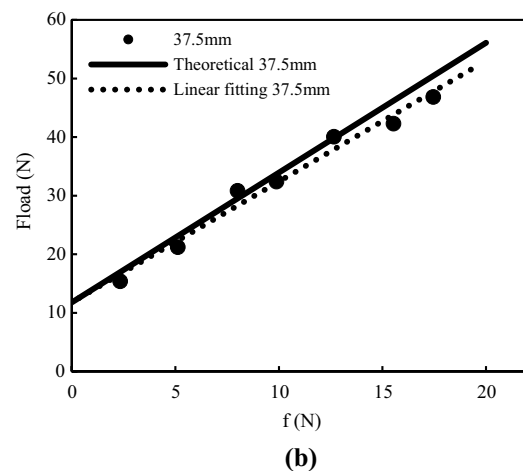
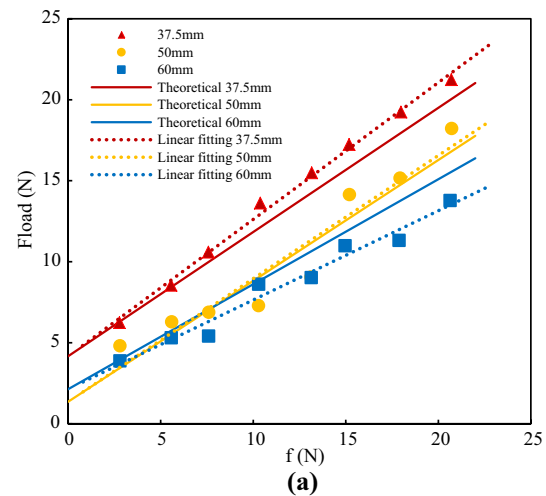
Two types of objects are prepared: (1) Rigid object: acrylic tube with radius of 37.5 mm, 50 mm and 60 mm is used. (2) Non-rigid object: it is made by pouring 0-degree (Shore hardness A) silica gel into a 3D printing mold with radius of 37.5 mm. The silica gel has tactile and mechanical properties close to the human body [25]. Figure 11b depicts the front perspective of the gripper gripping a non-rigid object with radius of 37.5 mm. The data acquisition system consists of four parts: rope tension sensor, loading force sensor, 24-bit ADC, STM32 MCU and a PC host computer. It can record the force acting on the sensors and transmit it to the PC through USB interface for further analysis.

Figure 11c shows the experimental process to verify the load capacity on a rigid object with radius of 50 mm. The specific experimental methods and steps are as follows: (1) place the objects in the gripper; (2) tighten the rope and apply the preconcerted tension on the rope; (3) change the loading force on the object by slowly pulling the object upward to imitate the workload; (4) record the rope tension and loading force until the object gets away from the gripper. And the load capacity of the gripper can be deduced.

Figure 11d shows the experimental process to verify the force transfer ratio on a non-rigid object with radius of 37.5 mm. In this paper, the grip force is indirectly measured by measuring the static friction. The specific experimental methods and steps are as follows: (1) prepare a ruler made by 304 stainless steel as the test middle piece; (2) clamp the ruler between the contact surfaces and slowly apply loading force parallel to the contact surface until the ruler starts to move; (3) record the loading curve and its peak value. The grip force between the contact surfaces can be deduced according to the static friction coefficient between materials.

## 5.2 The load capacity experiment

To verify the relationship between the rope tension and the load capacity, experiments on rigid object and non-rigid object are carried out. Figure 12 is part of the original data collected during the experiment. The dotted line is the rope tension and the solid line is the loading force during the



**Fig. 13** Comparison between the theoretical results and the experimental results of the load capacity on **a** the rigid acrylic objects and on **b** the non-rigid object

experiment. It can be seen that the rope tension is almost unchanged during the experiment. As the loading process goes on, the loading force slowly increases to a peak value and then decreases rapidly. This is due to the loading force reaching the maximum load capacity, and making the object gets away from the gripper. The original data were obtained by the above methods, and the following process was used to determine the load capacity.

(1) Summarize the peak value and perform Least Square Fitting Method to obtain the fitting line as the dotted line shown in Fig. 13.

(2) Take the friction coefficient  $\mu$  between part and the object (made of acrylic) as 0.05, and the friction coefficient  $\mu$  between part and the object (made of silica gel) as 0.5.

(3) The intercept of each dotted line on y-axis is obtained as the offset deviation of the system (i.e., caused by gravity). The slope of each dotted line is the load capacity ratio (load capacity per rope tension). Compared with the theoretical

results in Sect. 4, the load capacity ratio has a gain deviation of 1.61 (i.e., caused by friction in the gripper).

(4) To facilitate the comparison, multiply the theoretical result by the gain deviation of 1.61, and add the offset deviation to the result to obtain the theoretical results (with system error) as the solid line shown in Fig. 13.

From the above processing, the relationship between the rope tension and the load capacity can be obtained, as shown in Fig. 13. Figure 13a is the comparison between experimental results and the theoretical results performed on the rigid objects. The abscissa is the rope tension, and the ordinate is the load capacity. The solid line and the dotted line are respectively the theoretical results and the experimental results. The dotted lines are fitted from eight groups of experiments for each object when the rope tension changes from 2.5 N to 20 N. In the figure, marks '○', '△', '□' are used to distinguish objects with different radius.

Figure 13b shows the experimental results for the soft object with radius of 37.5 mm. The dotted line is fitted from seven groups of experiments when rope tension changes from 2.5 N to 17.5 N. The solid line, the abscissa and the ordinate are defined in the same way.

The following results can be obtained from Fig. 13a:

(1) The larger the radius of the object, the smaller the slope of the dotted line. It shows that, under the same rope tension, the larger the radius, the smaller the load capacity. This is in line with the theoretical results in Sect. 4.

(2) The slope of the dotted line is close to the solid line and changes with the radius of the object. However, the range of change is small, the reason is that, as shown in Eq. (8) and Eq. (10), when the radius of the object  $r$  is changing, both the contact position  $x_2, x_3$  and the arm of force of the rope tension around Distal and Central Joint will change.

(3) When the radius of the object is 37.5 mm, the dotted lines move up along the y-axis obviously compared with that of 50 mm. It shows that when the object is small, the movement of joints ( $\theta_2, \theta_3$ ) increases, which makes the arm of force of the link gravity around Distal Joint and Central Joint increase, resulting in the increase in the torque derived from the weight.

(4) Since the experimental conditions are not satisfactory, there are some random deviations between the data points and the lines.

The following results can be obtained from Fig. 13b:

(1) Similar to the results shown in Fig. 13a, the dotted line are close to the solid line.

(2) Compared with Fig. 13a, the most obvious difference in Fig. 13b is that the slope of the dotted line (the load capacity ratio) is significantly larger than that of the rigid objects. This result shows that when the object is non-rigid, the load capacity of the gripper is significantly larger than

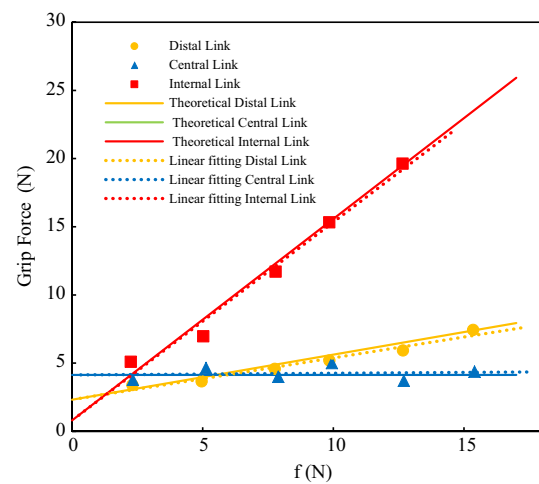


**Fig. 14** Comparison between the theoretical results and the experimental results of the grip force on the 37.5 mm non-rigid object

that of a rigid object, the main reason is the friction coefficient between the silica gel and the gripper is larger. In addition, the deformation of the non-rigid object increases the resistance between the gripper and the object.

(3) Compared with Fig. 13a, the data points in Fig. 13b are closer to the lines. This is because the friction coefficient between silica gel and gripper is significantly larger than that of the acrylic, which makes the contribution rate of the friction to load capacity up to 75% and reduces the relative error.

### 5.3 The force transfer ratio experiment

To verify the relationship between the rope tension and the grip force, the force transfer ratio experiment of each link is carried out as described in Sect. 5.1.

Figure 14 shows the comparisons between the theoretical results and the experimental results of the grip force on the non-rigid object with radius of 37.5 mm. Similarly, the theoretical results and the experimental results are obtained by the method mentioned in Sect. 5.2. In the figure, the abscissa is the rope tension and the ordinate is the grip force. The marks '○', '△', '□' are used to distinguish different links. The solid lines are the theoretical values and the dotted lines are the fitting lines obtained by the Linear Least Square Method. The slope of the lines that indicates the force transfer ratio (grip force per rope tension) of the gripper, is determined by the relationship between the rope tension and the grip force of each link.

The following conclusions can be drawn from Fig. 14:

(1) The grip force of the Central Link (marked as '△') is almost not affected by the rope tension. The reason is that all the driving force of the Central Joint is canceled by the

reacting force from the Distal Link when the spring is not installed. This result is consistent with the theoretical results.

(2) The force transfer ratio of the Internal Link (marked as '□') is significantly larger, this is because the Internal Joint is a translational joint, and there is no force amplification phenomenon caused by the Lever Principle.

(3) The slope of the dotted lines are close to the solid lines, due to the relatively large friction coefficient between the silica gel and the test ruler, the relative error is reduced.

The experimental results show that there are proportional relationships between the load capacity and the rope tension, as well as the grip force and the rope tension. This is consistent with the theoretical analysis in Sect.4. In particular, the load capacity of the non-rigid object is larger, which indicates that this kind of gripper is suitable for gripping a soft object, such as human limbs.

## 6 Summary

This paper proposes a bionic design for a universal gripper of the nursing robot. By analyzing the structure of a human hand and the operation law when gripping cylindrical objects with different sizes, we proposed the concept of Equivalent Link Length (ELL) to optimize the envelope effect. To increase gripping stiffness and avoid the harmful component widely contained in the grip force of fully rotational joints gripper, we proposed a single rope under-actuated architecture with hybrid rotational and translational joints.

Theoretical analysis and experiments to evaluate the performance of the structure are carried out on several aspects, such as envelope effect, force transfer ratio and load capacity. These results show that the proposed gripper can grasp objects with wide size range and has no harmful component in the grip force. Also, the force transfer ratio of the gripper is almost constant, which can reduce the number of sensors required by the system. And a load capacity of 2 N can be obtained for every 1 N of the rope tension when gripping a silica gel non-rigid object with radius of 37.5 mm. In addition, we found that the load capacity for the non-rigid object was significantly larger than that of the rigid one.

In future, we will continue to optimize the gripper's structure, such as coating the gripper fingers with malleable material, which will further increase the load capacity, and greatly help to reduce the size and the weight of the gripper.

**Authors' contributions** DX: Conceptualization, Methodology, Hardware and Software, Validation, Writing—original draft, Writing—review & editing. XL: Resources, Writing—review & editing, Project administration, Funding acquisition. YW: Validation, Writing—review & editing, Project administration.

**Funding** This work was supported by Key R & D project of Shandong Province [Grant No. 2019GGX104038] and Fundamental Research Funds of Shandong University [Grant No. 2016JC001].

## Declarations

**Conflict of interest** The authors have no conflicts of interest to declare that are relevant to the content of this article.

## References

- Greene J, Gibson DM (2021) Workers at long-term care facilities and their risk for severe covid-19 illness. *Prev Med* 143:106328. <https://doi.org/10.1016/j.ypmed.2020.106328>
- Yang GZ, Nelson BJ, Murphy RR, Choset H, Mcnutt M (2020) Combating covid-19 the role of robotics in managing public health and infectious diseases. *Sci Robot*. <https://doi.org/10.1126/scirobotics.abb5589>
- Yang G, Lv H, Zhang Z, Yang L, Yang H (2020) Keep healthcare workers safe: application of teleoperated robot in isolation ward for covid-19 prevention and control. *Chin J Mech Eng*. <https://doi.org/10.1186/s10033-020-00464-0>
- Park D, Hoshi Y, Mahajan HP, Kim HK, Erickson Z, Rogers WA, Kemp CC (2020) Toward active robot-assisted feeding with a general-purpose mobile manipulator: Design, evaluation, and lessons learned. *Robot Auton Syst*. <https://doi.org/10.1016/j.robot.2019.103344>
- Schroer S, Killmann I, Frank B, Vlker M, Burgard W (2015) An autonomous robotic assistant for drinking. *Proc IEEE Int Conf Robot Autom* 2015:6482–6487. <https://doi.org/10.1109/ICRA.2015.7140110>
- Mohanta JK, Mohan S, Wenger P, Chevallereau C (2021) A new sitting-type lower-limb rehabilitation robot based on a spatial parallel kinematic machine. In: Sen D, Mohan S, Ananthasuresh G (eds) *Mechanism and machine science. Lecture notes in mechanical engineering*. Springer, Singapore. [https://doi.org/10.1007/978-981-15-4477-4\\_54](https://doi.org/10.1007/978-981-15-4477-4_54)
- Ding M, Ikeura R, Mori Y, Mukai T, Hosoe S (2014) Lift-up motion generation of nursing-care assistant robot based on human muscle force and body softness estimation. In: *IEEE/ASME international conference on advanced intelligent mechatronics*. <https://doi.org/10.1109/AIM.2014.6878262>
- MingDing TakamitsuMatsubara, YoshihitoFunaki RyojunIkeura, ToshiharuMukai TsukasaOgasawara (2017) Generation of comfortable lifting motion for a human transfer assistant robot. *Int J Intell Robot Appl* 1:74–85. <https://doi.org/10.1007/s41315-016-0009-z>
- Home-life science robotics. <https://www.lifescience-robotics.com>. Accessed 22 Jan 2021
- Zhao Z, Li X, Lu C, Zhang M, Wang Y (2020) Compliant manipulation method for a nursing robot based on physical structure of human limb. *J Intell Rob Syst*. <https://doi.org/10.1007/s10846-020-01221-0>
- Victor G, Svetlana G, Bram V, Dirk L, Carlos RG (2017) Multi-axis force sensor for human-robot interaction sensing in a rehabilitation robotic device. *Sensors* 17:1294. <https://doi.org/10.3390/s17061294>
- Kahn LE, Zygmant ML, Rymer WZ, Reinkensmeyer DJ (2006) Robot-assisted reaching exercise promotes arm movement recovery in chronic hemiparetic stroke: a randomized controlled pilot study. *J Neuroeng Rehabil* 3:12. <https://doi.org/10.1186/1743-0003-3-12>

13. Zhang F, Hou ZG, Cheng L, Wang W, Chen Y, Hu J, Peng L, Wang H, Hou ZG (2016) ileg—a lower limb rehabilitation robot: a proof of concept. *IEEE Trans Hum-Mach Syst* 46:761–768. <https://doi.org/10.1109/THMS.2016.2562510>
14. Yu H, Huang S, Chen G, Pan Y, Guo Z (2015) Human-robot interaction control of rehabilitation robots with series elastic actuators. *IEEE Trans Rob* 31:1089–1100. <https://doi.org/10.1109/TRO.2015.2457314>
15. Clement R, Bugler K, Oliver C (2011) Bionic prosthetic hands: a review of present technology and future aspirations. *The Surgeon*. <https://doi.org/10.1016/j.surge.2011.06.001>
16. He Z, Yurievich RR, Shimizu S, Fukuda M, Kang Y, Shin D (2020) A design of anthropomorphic hand based on human finger anatomy. *IEEE*. <https://doi.org/10.1109/CcS49175.2020.9231423>
17. Rahman MF, Zhang K, Herrmann G (2019) Modular, underactuated anthropomorphic robot hand with flexible fingers and twisted string actuators. In: Althoefer K, Konstantinova J, Zhang K (eds) *Towards autonomous robotic systems. TAROS 2019. Lecture notes in computer science, vol 11650*. Springer, Cham. [https://doi.org/10.1007/978-3-030-25332-5\\_47](https://doi.org/10.1007/978-3-030-25332-5_47)
18. Deimel R, Brock O (2016) A novel type of compliant and underactuated robotic hand for dexterous grasping. *Int J Robot Res*. <https://doi.org/10.1177/0278364915592961>
19. Daniel M, Aukes B, Heyneman J, Ulmen H, Stuart, and M., (2014) Design and testing of a selectively compliant underactuated hand. *Int J Robot Res*. <https://doi.org/10.1177/0278364913518997>
20. Ciocarlie M, Hicks FM, Holmberg R, Hawke J, Schlicht M, Gee J, Stanford S, Bahadur R (2014) The velo gripper: a versatile single-actuator design for enveloping, parallel and fingertip grasps. *Int J Robot Res* 33:753–767. <https://doi.org/10.1177/0278364913519148>
21. Heidari H, Pouria MJ, Sharifi S, Karami M (2017) Design and fabrication of robotic gripper for grasping in minimizing contact force. *Adv Space Res* 61:1359–1370. <https://doi.org/10.1016/j.asr.2017.12.024>
22. Dong H, Asadi E, Qiu C, Dai J, Chen IM (2017) Geometric design optimization of an under-actuated tendon-driven robotic gripper. *Robot Comput-Integr Manuf*. <https://doi.org/10.1016/j.rcim.2017.09.012>
23. Choi H, Ko M (2006) Design and feasibility tests of a flexible gripper based on inflatable rubber pockets. *Int J Mach Tools Manuf* 46:1350–1361. <https://doi.org/10.1016/j.ijmachtools.2005.10.009>
24. Pettersson A, Davis S, Gray JO, Dodd TJ, Ohlsson T (2010) Design of a magnetorheological robot gripper for handling of delicate food products with varying shapes. *J Food Eng* 98:332–338. <https://doi.org/10.1016/j.jfoodeng.2009.11.020>
25. Mukherjee S, Chawla A, Karthikeyan B, Soni A (2007) Finite element crash simulations of the human body: passive and active muscle modelling. *Sadhana* 32:409–426. <https://doi.org/10.1007/s12046-007-0032-8>

**Publisher's Note** Springer Nature remains neutral with regard to jurisdictional claims in published maps and institutional affiliations.

Springer Nature or its licensor (e.g. a society or other partner) holds exclusive rights to this article under a publishing agreement with the author(s) or other rightsholder(s); author self-archiving of the accepted manuscript version of this article is solely governed by the terms of such publishing agreement and applicable law.